Volume 7
Number 10
26 May 2026
Pages 4931–5398

Materials Advances

rsc.li/materials-advances

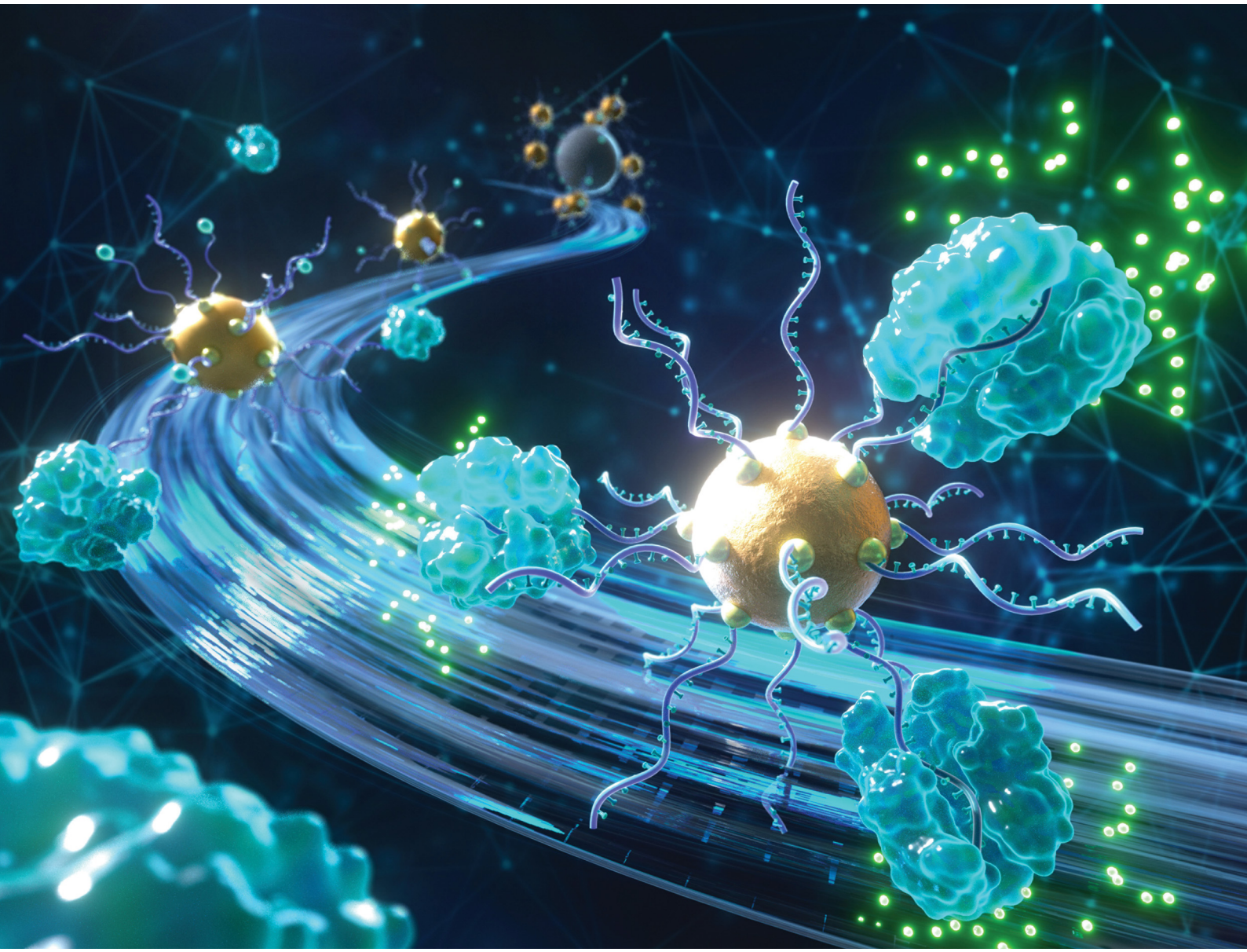

ISSN 2633-5409

ROYAL SOCIETY OF CHEMISTRY

PAPER
Haiyan Zheng, Xiyun Guan *et al.*
A CRISPR–Cas12a amplified RNase activity sensor powered by gold nanoparticle–barcode DNA multipliers

Materials Advances

ROYAL SOCIETY OF CHEMISTRY

PAPER

View Article Online
View Journal | View Issue

Cite this: *Mater. Adv.*, 2026, 7, 4973

A CRISPR–Cas12a amplified RNase activity sensor powered by gold nanoparticle–barcode DNA multipliers

Sathishkumar Munusamy, Rana Jahani, Jun Chen, Shuo Zhou, Juanhua Kong, Haiyan Zheng * and Xiyun Guan *

Received 6th March 2026,
Accepted 2nd April 2026

DOI: 10.1039/d6ma00316h

rsc.li/materials-advances

Ribonuclease A (RNase A) is a clinically relevant biomarker whose aberrant activity compromises RNA stability and interferes with RNA-based therapeutics, highlighting the need for rapid and ultrasensitive detection tools. In this work, we developed a CRISPR/Cas12a-assisted biosensing platform integrated with a substrate-bridged magnetic bead–gold nanoparticle assembly (SB-MAC) for highly sensitive and selective RNase A detection. By optimizing AuNP loading density, RNA substrate/barcode DNA molar ratio, and enzymatic incubation conditions, the prepared dual-functionalized SB-MAC architecture enabled efficient substrate/RNase A cleavage interaction and significant signal amplification, yielding a limit of detection (LOD) of 0.16 pg mL^{-1} for RNase A. The sensor exhibited excellent specificity against structurally and functionally related biomolecules and demonstrated strong analytical performance when tested on serum and water samples, with recoveries obtained ranging from 104 to 110%. Owing to its modular substrate design and robust signal amplification, this DNA-assisted platform offers a versatile and clinically relevant tool for monitoring RNase A activity and can be readily adapted for detecting other nuclease-based biomarkers.

Introduction

Ribonuclease A (RNase A) is a highly stable bovine pancreatic endoribonuclease that selectively cleaves cytosine- and uracil-containing RNA in ssRNA, dsRNA, and RNA–DNA hybrids.[1,2] Its disulfide-stabilized structure confers exceptional resistance to thermal and chemical degradation, making it a central model in enzymology and a widely used tool in molecular biology.[3] Beyond RNA metabolism, RNase A is involved in immune regulation, cellular proliferation, and host defense, and abnormal RNase A activity has been closely linked to pancreatic, ovarian, bladder, and thyroid cancers.[4–7] Its intrinsic cytotoxic and antiviral properties further elevate its biomedical relevance. Given these diverse functions, sensitive and accurate detection of RNase A activity is essential for early cancer diagnosis, therapeutic evaluation, and mechanistic studies. Meanwhile, the rapid expansion of RNA therapeutics, including mRNA vaccines and siRNA platforms,[8,9] demands stringent monitoring of RNase A contamination to preserve RNA integrity in research and manufacturing.

Gelatin zymography,[10] radioactive labeling,[11] and methylene blue[12] tests have long been the standard methods for measuring RNase A activity. However, the various limitations of these methods such as being time-consuming, expensive, and not very sensitive and suffering from hazardous radiation have severely restricted their practical applications. To overcome the constraints of classical RNase A activity assays, a number of new biosensing methodologies have been developed, including electrochemical and fluorescence-based approaches[13,14] as well as EtBr-mediated label-free platforms,[15] which convert the biological event (enzymatic cleavage of the substrate) into an electronic or optical signal. Although these methods offer more sensitive and convenient analysis, they still frequently require complex sample-handling procedures or sophisticated instrumentation.

Recently, the integration of various amplification techniques with highly specific biological recognition elements has significantly improved the limits of detection in the fields of diagnostics and biosensing, enabling the analysis of biomarkers at ultra-low concentrations. Amplified detection of enzymatic biomarkers commonly relies on signal-enhancing schemes such as nanoparticle-assisted probe release,[16,17] catalytic hairpin assembly (CHA),[18] rolling circle amplification (RCA),[19–21] and CRISPR–Cas-mediated collateral cleavage.[22–24] These strategies convert limited enzyme turnover into large, quantifiable outputs through catalytic recycling, structural rearrangement, or nuclease-driven signal cascades. As a result, such amplification modes substantially lower the detection

Department of Chemistry, University of Missouri, Columbia, MO, 65211, USA.
E-mail: haiyanzheng1111@gmail.com, xgpc2@missouri.edu

limits and improve robustness in complex samples. Despite their advantages, the current amplification techniques still face challenges. For example, CHA can exhibit slow reaction kinetics and occasional background leakage, necessitating careful sequence and buffer optimization, while RCA introduces additional operational steps due to its reliance on ligation and polymerase activity and may be susceptible to nonspecific priming. CRISPR–Cas-based amplification, although exceptionally sensitive, requires precise crRNA design and strict reaction control to minimize background from collateral cleavage and to ensure enzyme stability across different assay formats. Moreover, although CRISPR–Cas systems offer exceptional specificity, their collateral cleavage activity alone is not inherently sufficient for amplified detection, as the enzyme still requires a well-defined and purified DNA activator to initiate *trans*-cleavage. In complex biological samples, such target molecules may be scarce, masked by matrix components, or difficult to liberate without upstream processing. As a result, CRISPR often benefits from integration with complementary amplification modules such as nanoparticle-assisted probe release, which generate abundant, clean activator strands in response to enzyme activity. By coupling CRISPR with nanomaterial-enabled signal generation, the overall system could achieve greatly enhanced sensitivity and reliability, transforming modest biochemical events into robust and quantifiable readouts.

Due to their tunable optical properties, versatile surface chemistry, and excellent biocompatibility, gold nanoparticles (AuNPs) have been integrated into biological sensing platforms for detection of various biomolecules, including nucleases and RNA-degrading enzymes.[25–30] Many of these assays rely on changes in particle aggregation, surface charge, or hydrodynamic behavior upon substrate cleavage.[31,32] Although these approaches provide convenient readouts, their sensitivity is often limited by the direct signal output generated from a single enzymatic cleavage event and the intrinsic noise associated with nanomaterial aggregation phenomena. To overcome these constraints, strategies coupling AuNP-assisted substrate presentation with downstream signal amplification have gained increasing attention.[33–35] In this work, we introduce a fundamentally different and highly sensitive detection approach for RNase A activity measurement by exploiting dual-functionalized AuNPs to increase substrate loading density and convert each RNase A-mediated cleavage event into a large number of barcode DNA molecules. These DNA reporters subsequently activate CRISPR–Cas12a, enabling robust fluorescence amplification far beyond that achievable through traditional nanomaterial-based sensing. While CRISPR–Cas12a is widely recognized for nucleic acid detection, recent studies have demonstrated its adaptability for monitoring enzyme activities through rational substrate design, providing a powerful mechanism for translating biochemical reactions into amplified nucleic acid signals. The sensing strategy presented in this work establishes a generic framework for nuclease activity assays and offers strong potential for application in RNA therapeutic manufacturing, contamination monitoring, and minimally invasive clinical diagnostics.

Materials and methods

Materials

Streptavidin-coated magnetic beads (2.8 μm diameter, 10 mg mL^{-1}) were obtained from Invitrogen (Carlsbad, CA, USA), while 30 nm gold colloidal nanoparticles were purchased from Nanopartz (Loveland, CO, USA). LbCas12a, crRNA, and all the other DNA/RNA oligonucleotides, including the thiolated RNase A substrate, were synthesized by Integrated DNA Technologies (Coralville, IA, USA). All the enzymes and proteins, including RNase A, RNase H, DNase I, trypsin, thrombin, cathepsin-D, HIV protease, BSA, and HSA, were purchased from Sigma-Aldrich (St. Louis, MO, USA). All other chemicals and reagents were of analytical grade and used without further purification.

Engineering AuNPs with an RNA substrate and amplifier strands

Dual-functionalized AuNPs were prepared through thiol–gold surface conjugation using a dithiol-protected RNA substrate for RNase A (sequence: 5′-HS-S-$(CH_2)_6$-rCrUrGrUrGrCrGrUrGrUrGrArCrArGrCrGrGrCrUrGrA-TEG-biotin-3′, where TEG is a 15 atom tetraethylene glycol spacer) and a 20-mer dithiol-protected amplifier DNA strand (P1) with the sequence 5′-HS-S-$(CH_2)_6$-TTTTTTTTTTTTTTTTTTTT-3′. Both the substrate and P1 were individually reduced to generate free thiol groups prior to AuNP functionalization. Briefly, each oligonucleotide solution was incubated separately with TCEP (tris(2-carboxyethyl)phosphine) for 1 h at ambient temperature to cleave the disulfide protection and release reactive thiol moieties. These freshly reduced oligonucleotide stocks were then used to prepare the functionalization premixes. To control the surface loading composition, the substrate and P1 were combined at molar ratios of 1 : 25, 1 : 50, 1 : 100, and 1 : 200. Each premix was prepared at a total oligonucleotide concentration of 50 μM in a final volume of 50 μL, optimized for modification of 100 μL of 35 nM citrate-stabilized AuNPs. For functionalization, 100 μL of AuNPs was gently mixed with the corresponding 50 μL ligand premix and allowed to react for 1 h at room temperature with intermittent mixing to promote efficient Au–S binding. To enhance ligand packing density, an aging–salting process[36] was applied by gradually increasing the NaCl concentration to 0.3 M using a 2 M NaCl stock, followed by overnight incubation. Functionalized AuNPs were purified by centrifugation at 10 000*g* for 10 min, washed, and resuspended in PBS containing 0.1% Tween-20. The total oligonucleotide loading for each substrate/P1 ratio was quantified using UV-vis absorbance measurements. Specifically, oligonucleotide uptake was determined by comparing the absorbance of a control solution containing the same concentration and volume of free oligonucleotides (without AuNPs) with the absorbance of the supernatant collected after centrifugation of the AuNP–oligonucleotide conjugates.[37] The decrease in the absorbance of the supernatant relative to the control corresponded to the amount of oligonucleotide immobilized on the AuNP surface (SI, Fig. S1).

Preparation of streptavidin-coated MBs

Before conjugation, streptavidin-coated magnetic beads (MBs; Dynabeads™ M-280 Streptavidin, 10 mg mL^{-1}) were blocked

with 0.1% bovine serum albumin (BSA) to reduce nonspecific interactions. Briefly, 100 μL of the MB suspension was blocked with BSA, washed with phosphate-buffered saline (PBS), and then diluted with PBS to a final volume of 1 mL. A fixed amount of 10 μL was used for all the remaining experiments.

Assembly of substrate-linked MB–AuNP constructs

For the assembly of the substrate-bridged magnetic bead–AuNP complex (SB-MAC), 10 μL of streptavidin-coated magnetic beads (pretreated with 0.1% BSA) was washed and resuspended in 100 μL of PBS containing 0.1% Tween-20 (PBST). This suspension served as the binding buffer for AuNP attachment. To construct each SB-MAC variant, 5 μL of dual-functionalized AuNPs, which were prepared individually using one of the predefined RNA substrate/P1 molar ratios (1 : 25, 1 : 50, 1 : 100, or 1 : 200), was added to the bead suspension. The mixture was briefly vortexed and gently agitated for 30 min at room temperature to facilitate efficient biotin–streptavidin coupling between the RNA substrate on the AuNPs and the surface of the magnetic beads. After incubation, the AuNP-decorated beads were magnetically separated and washed three times with PBST (PBS + 0.1% Tween-20) to remove unbound nanoparticles. The purified SB-MAC constructs corresponding to each specific functionalization ratio were finally resuspended in PBS and stored at 4 °C until use in RNase A digestion and subsequent CRISPR/Cas12a fluorescence analysis.

Procedure for CRISPR-assisted detection of RNase A *via* SB-MAC digestion

Following successful assembly, the SB-MAC complexes were resuspended in 1 mL of RNase A reaction buffer (consisting of 0.1 M NaCl, 2.5 mM Mg^{2+}, and 5 mM Tris, pH 7.5) and equilibrated at 37 °C. RNase A at various concentrations ranging from 0.5 to 100 pg mL^{-1} was then introduced, and the mixture was incubated at 37 °C for 30 min with gentle agitation to allow enzymatic digestion of the RNA substrate and release of DNA activators into solution. Next, the magnetic beads were separated using a magnetic rack, and the bead-free supernatant was collected, 100 μL of which was used for subsequent CRISPR/Cas12a analysis. In parallel, the Cas12a–crRNA complex was prepared separately by incubating Cas12a (4 μL, 1 μM) with the corresponding crRNA (sequence: rUrArArUrUrUrCrUrArCrUrArArGrUrGrUrArGrArUrArArArArArArArArArArArArArArArATATTATT, 6 μL, 2 μM) in 1× NEBuffer 2.1 (20 μL) at room temperature for 30 min. To initiate the CRISPR reaction, the collected 100 μL of bead-free supernatant, 10 μL of FAM/quencher-labeled ssDNA reporter (sequence: FAM-TTATT-IABkFQ, 5 μM), and the preformed Cas12a-crRNA complex were incubated at room temperature for 3 h, allowing collateral cleavage–driven fluorescence signal generation. Fluorescence measurements were then recorded at an excitation/emission wavelength of approximately 490/521 nm using a fluorescence spectrophotometer.

Results and discussion

Working mechanism of the RNase A detection platform

In this work, a highly specific and ultrasensitive RNase A detection platform was developed by integrating dually functionalized AuNPs, streptavidin-coated magnetic beads (MBs), and CRISPR–Cas12a signal amplification (Fig. 1A and B). The

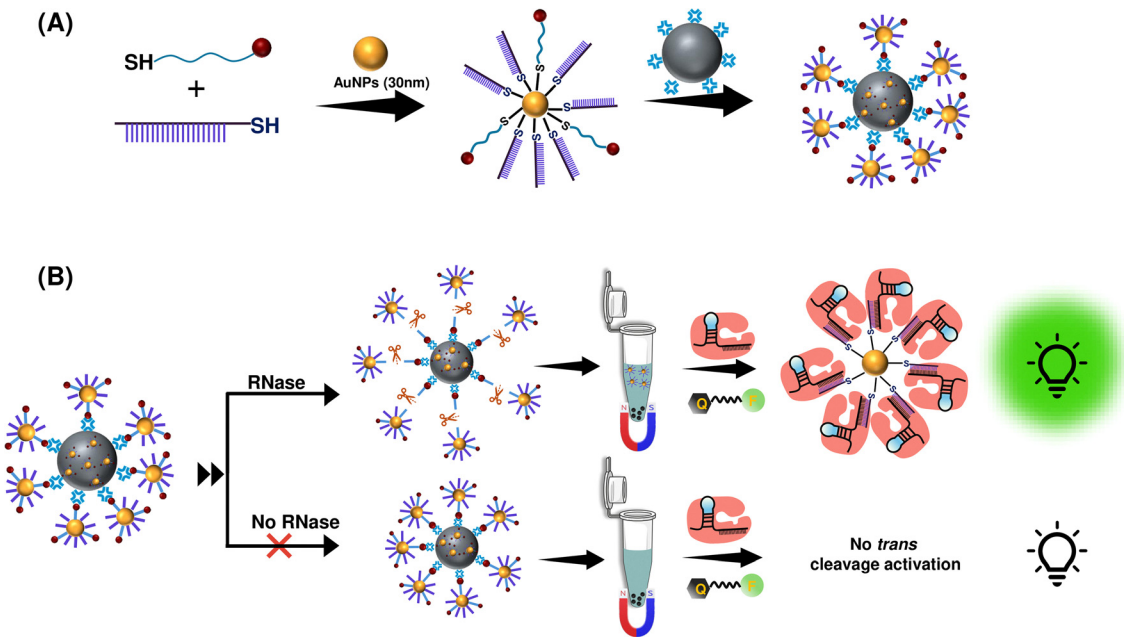

Fig. 1 Schematic illustration of the RNase A detection platform based on a substrate-bridged MB–AuNP assembly and CRISPR–Cas12a signal amplification. (A) Preparation of the functionalized MB reporter construct through biotin–streptavidin–mediated assembly of dually functionalized AuNPs carrying an RNase A–cleavable RNA substrate and DNA activator strands. (B) Cleavage-triggered AuNP release and DNA-assisted CRISPR–Cas12a enhancement strategy for RNase A detection, where RNase A-mediated substrate hydrolysis liberates activator-rich AuNPs, leading to Cas12a *trans*-cleavage activation and amplified fluorescence signal generation (not to scale).

design begins with the construction of an RNase A–cleavable substrate engineered with a biotin group at one terminus and a thiol group at the other. In parallel, a thiolated oligonucleotide activator (for downstream CRISPR analysis) is employed as a secondary DNA component to provide strong amplification capability. Initially, AuNPs are dually functionalized with the RNase A-specific substrate and the thiolated activator sequence to generate a hybrid nano-construct capable of both target recognition and signal amplification. These modified AuNPs are subsequently assembled onto streptavidin-functionalized MBs through the biotinylated end of the RNase A substrate, forming a robust reporter complex in which the substrate strand acts as a molecular ''bridge'' anchoring the AuNPs to the MB surface. After successful assembly, the complexes are washed to remove unbound materials and enriched to ensure high structural uniformity. Upon introduction of RNase A at varying concentrations, the enzyme selectively cleaves the substrate strand, disrupting the linkage between the AuNPs and MBs. This cleavage event releases the AuNPs, which can then be efficiently separated from the MBs using an external magnetic field. Notably, each released AuNP carries hundreds of activator strands, enabling significant signal enhancement. The liberated activator-rich AuNPs subsequently activate the CRISPR–Cas12a system programmed with a complementary guide RNA. In the presence of a target-derived activator, Cas12a is activated, thus cleaving the fluorescent reporter DNA and generating a strong fluorescence signal. Samples lacking RNase A retain the intact reporter complex, and hence, no AuNPs would be released into the solution, leading to background level fluorescence output. This modular workflow, which combines selective enzymatic cleavage, magnetic separation, and CRISPR-driven amplification, provides a powerful and cost-effective strategy for sensitive and highly specific detection of RNase A.

Verification of RNase A–substrate cleavage interaction by nanopore analysis

RNase A is a well-characterized endoribonuclease that catalyzes the cleavage of RNA at the 3′-side of pyrimidine residues, most notably cytosine (C) and uracil (U), within single-stranded, double-stranded, and RNA–DNA hybrid architectures. Inspired by this intrinsic substrate tolerance, we designed a 5′-thiol/3′-biotin-terminated RNA oligonucleotide (sequence: 5′-HS-$(CH_2)_6$-rCrUrGrUrGrCrGrUrGrUrGrArCrArGrCrGrGrCrUrGrA-TEG-biotin-3′) as the RNase A-responsive linker for our sensor assembly. This sequence incorporates multiple rC and rU residues, ensuring sufficient recognition sites for RNase A-mediated hydrolysis. Given the approximate molecular dimensions of RNase A (3.8 × 2.8 × 2.3 nm) and the estimated extended contour length of the engineered RNA substrate (~16 nm), we hypothesized that the enzyme would retain access to the cleavage motifs even when the substrate is immobilized between two nanoscale surfaces (*i.e.*, its 3′-biotin terminus bound to streptavidin-coated magnetic beads and its 5′-thiolated end anchored onto the surface of AuNPs). Although steric crowding at solid interfaces can compromise enzymatic turnover, it is expected that the substantial flexibility and length of the RNA strand, coupled with the small size of RNase A, still enable the enzyme's productive binding and catalysis.

To validate the feasibility of using the designed RNA substrate for RNase A detection, single molecule nanopore analysis of the cleavage interaction between the substrate and RNase A was first carried out. By monitoring ionic current fluctuations as individual molecules translocate or interact within the confined geometry of a nano-channel, nanopore technology has emerged as a versatile label-free tool to investigate various applications, including DNA sequencing,[38] biosensing,[39,40] investigating enzyme kinetics,[41,42] studying molecular interaction,[43,44] and so on. Owing to its high sensitivity and excellent resolution, nanopore technology is very useful to study short nucleic acid/peptide cleavage at low concentrations.[41,45] Our experimental results showed that the substrate alone in the $(M117F)_7$ α-hemolysin nanopore produced one major type of event with ~90% of full channel block and a large spread of residence time ranging from hundreds of microseconds to hundreds of milliseconds. However, in the presence of RNase A, the frequency of the long-lived events decreased significantly, and the majority of the events showed a residence time between ~0.3 and 3 ms (Fig. 2), confirming that the enzymatic reaction occurred. It should be noted that, in our sensor design, RNase A cleaves the RNA substrate, separating the AuNPs from magnetic beads, while the barcoding DNA on the AuNPs (sequence: TTTTTTTTTTTTTTTTTTTT) activates the Cas12a by base pairing with the highlighted region of the crRNA (rUrArArUrUrUrCrUrArCrUrArArGrUrGrUrArGrArUrArArArArArArArArArArArArArArArArArATATTATT), thus cleaving the dye-labeled reporter DNA (FAM-TTATT-IABkFQ), emitting fluorescence. The ability of Cas12a to cleave reporter DNA has been confirmed in our previous studies.[46] Since each RNase A–RNA cleavage event corresponds to multiple barcoding DNAs, a significant amplification in the analyte signal would be produced.

Material characterization and feasibility analysis

To demonstrate the feasibility of utilizing the sensing system for highly sensitive RNase A detection, initial experiments were performed by incubating AuNPs of 30 nm size with the RNA substrate/P1 mixture in a molar ratio of 1 : 50 to prepare dual functionalized AuNPs. Successful uptake of P1 and RNA on AuNPs was confirmed using UV-vis spectroscopy. Specifically, the characteristic absorbance of nucleic acids at 266 nm was monitored by comparing the spectrum of a control solution containing free RNA substrate and P1 with that of the supernatant collected after centrifugation of the functionalized AuNPs. A pronounced decrease in the absorbance of the supernatant relative to the control indicated effective immobilization of both the RNA substrate and P1 onto the AuNP surface, with the loading density determined to be 821 nucleic acid molecules per AuNP (SI, Fig. S1), confirming successful dual functionalization. Furthermore, the successful dual functionalization of AuNPs and retention of colloidal stability were also studied and characterized by transmission electron microscopy (TEM), zeta potential measurements and dynamic light scattering (DLS) analysis. Briefly, as shown in Fig. 3A and B, the citrate-stabilized

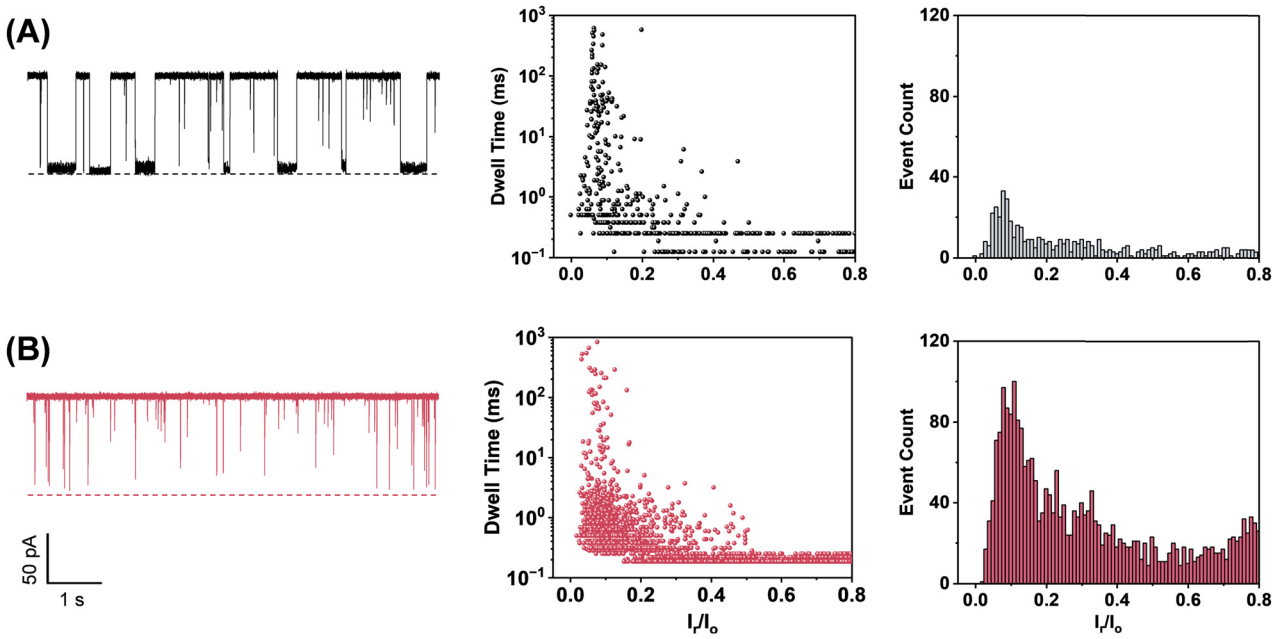

Fig. 2 Nanopore analysis of RNase A–RNA substrate cleavage interaction. (A) RNA substrate alone and (B) RNA substrate + RNase A. (Left) Representative single-channel recording trace segments; (middle) the corresponding scatter plots of event amplitude *versus* residence time; and (right) the event-list histograms. The experiments were carried out at + 120 mV using a $(M117F)_7$ α-hemolysin protein pore in an electrolyte solution containing 1 M NaCl and 10 mM Tris (pH 7.5). Both the RNA substrate and the RNA–RNase A mixture were added to the *cis* chamber compartment. As shown in Fig. 2B, the RNA–RNase A mixture was incubated in a 1 M NaCl electrolyte solution for 30 minutes before being analyzed by the nanopore. Scatter plots and event-list histograms were obtained based on 10 min trace segments. The concentrations of RNA and RNase A used were 0.5 μM and 2 ng mL^{-1}, respectively.

AuNPs exhibited uniform, well-dispersed spherical particles with smooth edges and consistent size distribution. Following functionalization with the RNase A–cleavable RNA substrate and the thiolated activator DNA, the TEM images revealed similarly well-dispersed particles but with a noticeably (~1.3 nm) increased diameter, indicating the successful formation of a surface-bound biomolecular layer (Fig. 3C and D). This size augmentation was further corroborated by DLS, which showed an appreciable increase (from 36 nm to 53 nm) in the hydrodynamic diameter after modification (Fig. 3E). Surface charge analysis provided additional confirmation of successful functionalization. For example, citrate-capped AuNPs initially displayed a strongly negative zeta potential (−46.2 mV), attributed to the deprotonated citrate groups. Upon introduction of the thiolated DNA components, the zeta potential shifted to −50.8 mV, reflecting the incorporation of negatively charged oligonucleotides on the AuNP surface (Fig. 3F). Taken together, the TEM, DLS, and zeta potential measurements collectively verify the effective functionalization and colloidal stability of the engineered AuNP nanoconstructs. Following functionalization, the engineered AuNPs were immobilized onto streptavidin-coated magnetic beads (MBs) *via* the strong biotin–streptavidin interaction to generate the substrate-bridged MB–AuNP complex (SB-MAC), as illustrated in Fig. 1. The formation of SB-MAC was verified by zeta potential measurements. As shown in Fig. S2 (SI), bare streptavidin-coated MBs exhibited a surface potential of −4.2 mV, consistent with their native surface chemistry. Upon conjugation with the negatively charged DNA-functionalized AuNPs, the zeta potential shifted to −7.6 mV, supporting the successful immobilization of AuNPs onto the MBs.

To evaluate the functional performance of the sensing platform, the prepared SB-MAC (10 μL) was introduced into 1 mL of the reaction buffer, followed by the addition of RNase A at a final concentration of 50 pg mL^{-1}. The mixture was then incubated for 30 min at 37 °C on a thermoshaker to allow RNase A-mediated cleavage of the RNA substrate. After incubation, the MBs were isolated using a magnetic rack, and the supernatant, which contained the released AuNPs upon substrate hydrolysis, was collected for downstream CRISPR analysis. For CRISPR activation, Cas12a was complexed with a guide RNA complementary to the activator sequence tethered on the AuNPs. A fluorogenic ssDNA reporter labeled with a FAM fluorophore and a quencher separated by five nucleotides served as the *trans*-cleavage substrate. Upon addition of the supernatant, samples containing RNase A exhibited a pronounced fluorescence enhancement, consistent with the release of activator-loaded AuNPs and subsequent activation of Cas12a (Fig. 4A). To confirm the specificity of the fluorescence response, a series of control experiments were systematically performed. These included SB-MAC samples incubated in the absence of RNase A, which retained the AuNPs on the bead surface and hence failed to activate Cas12a, and various CRISPR reaction mixtures. All control conditions resulted in much smaller fluorescence signals than the RNase sample, demonstrating that Cas12a activation occurs only when RNase A cleaves the RNA linker within SB-MAC and liberates the AuNP-bound activator in solution (Fig. 4B). Moreover, the supernatants

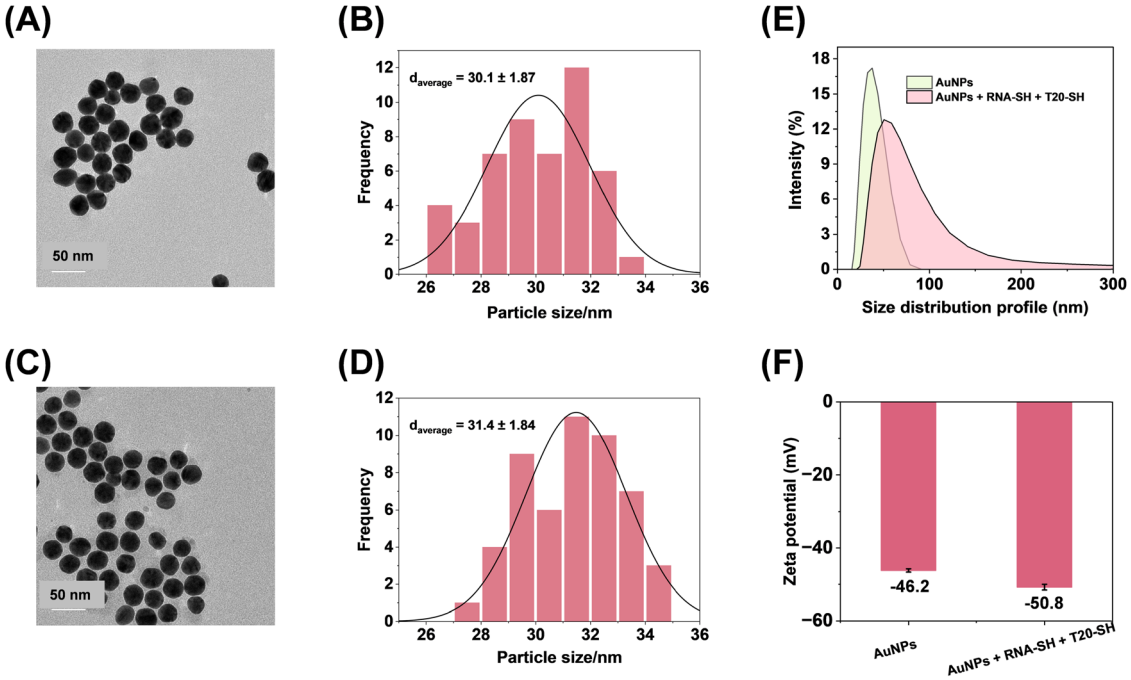

Fig. 3 Characterization of dual-functionalized AuNPs. (A) Representative TEM image and (B) size distribution of citrate-capped AuNPs. (C) Representative TEM image and (D) size distribution of AuNPs functionalized with both the RNase A–cleavable substrate and T20 amplifier (P1). (E) Dynamic light scattering (DLS) profiles of bare and functionalized AuNPs, showing an increase in the hydrodynamic diameter after dual functionalization. (F) Zeta potential analysis of AuNPs before and after functionalization, indicating enhanced negative surface charge, consistent with successful DNA immobilization and preserved colloidal stability. TEM images were acquired using a JEOL JEM-1400 instrument operated at 120 kV.

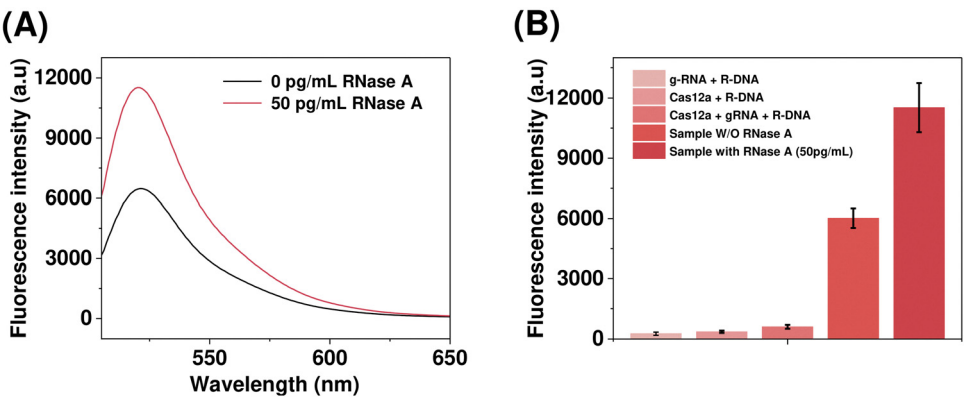

Fig. 4 (A) Fluorescence spectra showing Cas12a activation in the presence of RNase A (50 pg mL^{-1}), reflecting SB-MAC cleavage and releasing the activator-loaded AuNPs. (B) Fluorescence comparison of the RNase A sample with multiple controls. R-DNA and g-RNA represent the reporter ssDNA and guide RNA, respectively.

of freshly prepared SB-MAC assemblies and those stored at 4 °C for up to 7 days were analyzed using the CRISPR system. No significant differences in fluorescence intensity were observed between these samples (SI, Fig. S3), indicating that the SB-MAC assemblies remained highly stable during storage, with no detectable dissociation of the functionalized AuNPs or barcode DNA. In addition, the fluorescence signals obtained from these supernatant samples were significantly lower than those of the blank control (*i.e.*, the sample without RNase A). These results suggest that the detectable fluorescence observed in the absence of RNase A is likely attributed to weak nonspecific interactions between DNA-functionalized AuNPs and the magnetic bead surface. During incubation at elevated temperatures and subsequent magnetic separation, a small fraction of AuNPs may detach from the bead surface due to combined electrostatic repulsion, van der Waals forces, and mechanical agitation, even in the absence of enzymatic cleavage.[47] This nonspecific release results in a modest background signal, which remains negligible compared to the pronounced fluorescence enhancement induced by RNase A-mediated substrate cleavage. Therefore, the results demonstrate that the designed platform exhibits excellent operational fidelity: only the correct biochemical sequence—RNase A-dependent SB-

MAC disassembly followed by Cas12a activation—generates a measurable signal. This stringent response behavior validates the system as a highly selective and ultrasensitive sensor for RNase A detection.

Optimization of the experimental conditions

To improve the sensor performance, we next conducted systematic optimization of several key experimental parameters. Briefly, to investigate the effect of the loading density of dual-functionalized AuNPs on the surface of magnetic beads on RNase A detection, a series of SB-MAC assemblies were prepared by incubating dual-functionalized AuNPs at different concentrations ranging from 0.32 to 1.6 nM with a fixed concentration of MBs. The resulting AuNP-decorated MB complexes were then used to detect 50 pg mL^{-1} of RNase A. We found that increasing the concentration of used dual-functionalized AuNPs from 0.32 to 0.8 nM resulted in only a marginal enhancement in the fluorescence signal-to-noise ratio (SNR). Further increasing the AuNP concentration beyond 0.8 nM did not yield any significant improvement in SNR (Fig. 5A). Thus, 0.8 nM was deemed the optimum AuNP concentration for preparing the SB-MAC assembly, and this concentration was used in the subsequent experiments.

Another important parameter governing the sensitivity of the sensing system is the molar ratio of the P1 strand to the RNA substrate immobilized on AuNPs. In principle, as the ratio increases, a larger signal amplification per enzymatic cleavage event will be expected, leading to an increase in the generated fluorescence intensity. To investigate the molar ratio effect, a series of dual functionalized AuNPs were prepared by incubating AuNPs of 30 nm diameter with various P1/RNase A substrate mixtures in molar ratios ranging from 25 : 1 to 200 : 1. These dual-functionalized AuNPs were then coupled with MBs to form the SB-MAC assemblies. After addition of 50 pg mL^{-1} RNase A, the collected supernatants were subjected to CRISPR analysis. The largest sensor sensitivity (in terms of SNR) was observed at an RNA substrate/P1 molar ratio of 1 : 50, with both lower and higher P1 loadings leading to suboptimal responses (Fig. 5B). The results are not unreasonable considering that a too low substrate density on AuNPs might lead to a consequence that the crowdy P1 molecules would likely create a dense "corona" around the gold nanoparticles, effectively shielding the too low density substrates from the target RNase A. This would lead to a reduction in the desired enzymatic reaction, negatively impacting the sensor sensitivity. Moreover, the effect of incubation time on RNase A-mediated substrate digestion was also examined. 30 min was identified as the optimum incubation time and used in the subsequent experiments, beyond which no further improvement in signal output was observed (Fig. 5C).

Sensitivity and selectivity studies

With the key experimental parameters systematically optimized to ensure maximal assay performance, we next evaluated the analytical capabilities of the developed biosensing platform. To construct a dose–response curve, a series of RNase A solutions with concentrations ranging from 0.5 to 100 pg mL^{-1} were analyzed by using the DNA-assisted CRISPR–Cas12a sensing platform. We found that an increase in the RNase A concentration led to an increase in the fluorescence intensity (Fig. 6A). A strong linear relationship ($y = 110x + 6099$, $R^2 = 0.9682$) was observed between the fluorescence intensity at 521 nm and the RNase A concentration. Reproducibility was evaluated using nine independent measurements, encompassing both batch-to-batch and day-to-day variabilities. The corresponding reproducibility metrics and confidence intervals of fits are summarized in Fig. S4 and S5 in the SI. Based on the 3σ criterion,[48,49] the detection limit of the method was determined to be 0.16 pg mL^{-1} (Fig. 6B). As far as we are aware, such a detection limit is notably lower than various highly sensitive RNase A assays reported thus far (SI, Table S1). To assess the sensor selectivity, the DNA-assisted platform was further used to analyze a panel of potentially interfering biomolecules commonly present in biological matrices, including BSA, HSA, thrombin, cathepsin-D, RNase H, DNase, HIV-1 protease (HIV-1 PR), and trypsin at concentrations tenfold higher than the target RNase A. In all cases, much smaller fluorescence responses than RNase A were observed, confirming that only RNase A-mediated substrate digestion

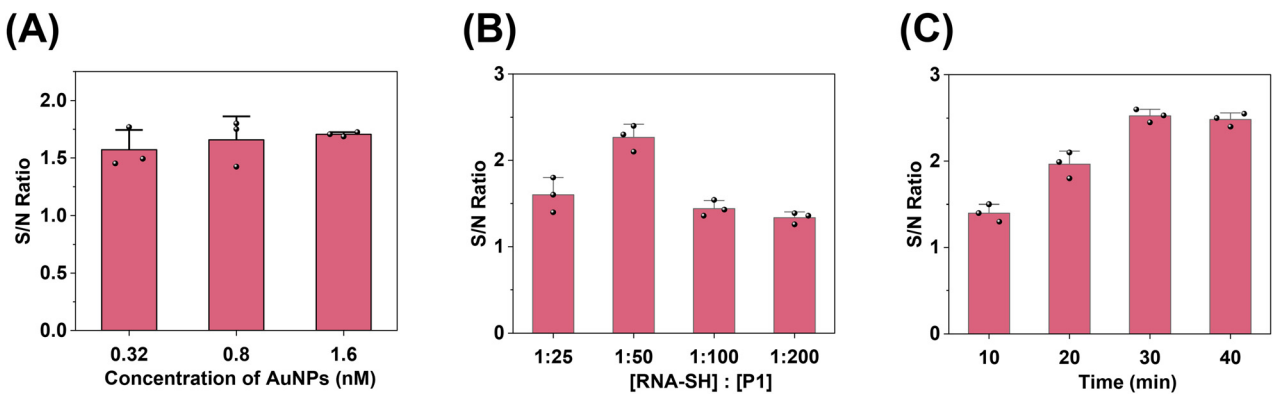

Fig. 5 Optimization of experimental conditions for RNase A detection. (A) Fluorescence responses of SB-MAC assemblies prepared with 0.32, 0.8, and 1.6 nM AuNPs to RNase A, showing signal saturation above 0.8 nM. Effects of (B) molar ratio of RNA substrate to P1 and (C) incubation time on CRISPR analysis readout. The concentration of RNase A used in Fig. 5 was 50 pg mL^{-1} each. Each data point represents the mean ± standard deviation from three independent replicates.

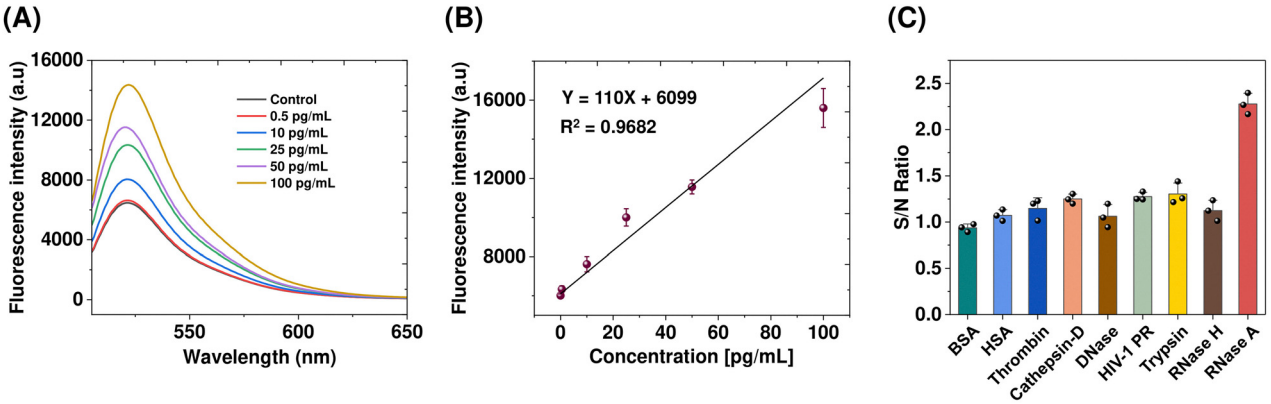

Fig. 6 (A) Fluorescence spectra of the SB-MAC system upon titration with varying concentrations of RNase A (0.5–100 pg mL^{-1}); (B) dose–response curve, showing the effect of RNase A concentration on the CRISPR-activated fluorescence signal; and (C) sensor selectivity. The fluorescence response in (A) was recorded using an excitation wavelength of 490 nm and an emission maximum at 521 nm, corresponding to the characteristic output of the CRISPR/Cas12a *trans*-cleavage reporter. The fluorescence intensity values shown in (B) were derived from the fluorescence spectra at 521 nm of (A). In (C), except for RNase A (at 50 pg mL^{-1}), the concentrations of all the other enzymes or proteins used were 500 pg mL^{-1} each. Data represent the mean ± standard deviation from three independent replicates.

triggers efficient Cas12a activation (Fig. 6C). Note that the high selectivity of the sensor is attributed to the structural fidelity of the RNA substrate and the stringent recognition characteristics of Cas12a.

Serum and water sample analysis

To further assess the practical applicability of our developed RNase A sensing platform in clinical diagnosis and RNase contamination monitoring, serum and water samples were analyzed using the optimized SB-MAC/CRISPR assay. The samples include serum from a healthy male and RNase-free water (both obtained from Sigma-Aldrich, St. Louis, MO), tap water from our chemistry building, and reaction buffer consisting of 10 mM Tris and 1 M NaCl (pH 7.5) commonly used in our laboratory. Except for the serum sample, which was analyzed after a 50-fold dilution with PBS buffer, all other samples were analyzed directly without any prior treatment. No appreciable fluorescence response beyond background levels was observed, indicating that these samples did not contain RNase A. To evaluate matrix effects and the accuracy of the platform, spike-and-recovery experiments were next performed, where defined concentrations of RNase A standards (0.5–50 pg mL^{-1}) were spiked into the diluted (1 : 50) serum and water. The measured concentrations and the corresponding recoveries are summarized in Table 1. Clearly, the sensor exhibited excellent quantitative performance for all the spiked samples, with recoveries obtained ranging from 104% to 110%, indicating minimal interference from the matrix components.

Table 1 Analysis of serum and water samples with the developed RNase A assay

Sample no.	Sample content	RNase A found[a] (pg mL^{-1})	Recovery (%)
1	Serum only	nd[b]	—
2	RNase-free water only	nd	—
3	Tap water only	nd	—
4	Reaction buffer only	nd	—
5	Serum + 0.5 pg mL^{-1} RNase A	0.52 ± 0.01	110 ± 2
6	Serum + 10 pg mL^{-1} RNase A	10.4 ± 0.4	104 ± 4
7	Serum + 25 pg mL^{-1} RNase A	26.1 ± 0.5	104 ± 2
8	Serum + 50 pg mL^{-1} RNase A	52.1 ± 1.8	104 ± 3
9	Tap water + 50 pg mL^{-1} RNase A	53.0 ± 2.6	106 ± 5

[a] Each value represents the mean of three replicate analyses ± one standard deviation. [b] nd: not detected.

Conclusions

In summary, we have constructed a highly sensitive and selective CRISPR-assisted biosensing platform for RNase A detection by integrating a substrate-bridged magnetic bead–gold nanoparticle complex (SB-MAC) with Cas12a-mediated signal amplification. Through systematic optimization of AuNP loading, RNA substrate/barcoding DNA molar ratio, and enzymatic incubation conditions, the sensor achieved a LOD of 0.16 pg mL^{-1}, outperforming the existing RNase A assays. The platform also exhibited excellent selectivity, showing negligible interference from structurally and functionally related biomolecules, underscoring the inherent molecular specificity of the engineered RNA substrate and the stringent recognition fidelity of Cas12a. Moreover, simulated serum and water samples were successfully analyzed, with the recovery obtained ranging from 104% to 110%. Beyond detecting RNase A, the modularity of the SB-MAC architecture allows easy adaptation to other nucleases or protease biomarker species by rational redesign of the substrate, thus offering a generic platform for developing next-generation enzymatic activity sensors. Looking forward, the platform may be expanded to high-throughput or multiplexed formats using bead arrays or microplate-based assemblies, providing a powerful analytical tool for disease diagnostics, therapeutic monitoring, and broader biochemical research.

Author contributions

Sathishkumar Munusamy: investigation, methodology, data curation, formal analysis, and writing – original draft. Rana Jahani: investigation. Jun Chen: investigation. Juanhua Kong: investigation. Shuo Zhou: investigation. Haiyan Zheng: writing – review & editing. Xiyun Guan: conceptualization, supervision, project administration, and writing – review & editing.

Conflicts of interest

The authors declare that they have no known competing financial interests or personal relationships that could have appeared to influence the work reported in this paper.

Data availability

Data will be made available upon request from the authors.

Supplementary information (SI): additional table and figures, including quantification of oligonucleotide loading on AuNPs, zeta potential of streptavidin-coated magnetic beads before and after AuNP conjugation, stability study of the prepared SB-MAC assemblies, reproducibility study of the DNA-assisted CRISPR–Cas12a sensing platform, relationship between fluorescence intensity and RNase A concentration, and performance comparison of the developed RNase activity assay with other reported detection methods. See DOI: https://doi.org/10.1039/d6ma00316h.

Acknowledgements

This work was financially supported by the National Institutes of Health (R01GM147247) and the National Science Foundation (2345813).

References

1 W. Dang, R. Luo, J. Fan, Y. Long, C. Tong, F. Xiao, X. Xiong and B. Liu, *Talanta*, 2020, **209**, 120512.
2 S. Talluri, D. M. Rothwarf and H. A. Scheraga, *Biochemistry*, 1994, **33**, 10437–10449.
3 T. A. Klink, K. J. Woycechowsky, K. M. Taylor and R. T. Raines, *Eur. J. Biochem.*, 2000, **267**, 566–572.
4 D. Sun, C. Han and J. Sheng, *iScience*, 2022, **25**, 105284.
5 Y. A. Siraj, *Transl. Med. Commun.*, 2022, **7**, 5.
6 C. Liu, C. Zhou, W. Xia, Y. Zhou, Y. Qiu, J. Weng, Q. Zhou, W. Chen, Y.-N. Wang, H.-H. Lee, S.-C. Wang, M. Kuang, D. Yu, N. Ren and M.-C. Hung, *Nat. Commun.*, 2024, **15**, 1009.
7 Z. Zha, C. Liu, M. Yan, C. Chen, C. Yu, Y. Chen, C. Zhou, L. Li, Y.-C. Li, H. Yamaguchi, L. Ye, T. Liu, Y.-N. Wang, H.-H. Lee, W.-H. Yang, L.-C. Chan, B. Ke, J. L. Hsu, L. Ding, D. Ji, P. Pan, Y. Meng, Y. Pu, L. Liu and M.-C. Hung, *Signal Transduction Targeted Ther.*, 2025, **10**, 124.
8 Y. Shi, M. Shi, Y. Wang and J. You, *Signal Transduction Targeted Ther.*, 2024, **9**, 322.
9 C. A. Freije and V. Arechavala-Gomeza, *Commun. Med.*, 2025, **5**, 463.
10 T. Yasuda, D. Nadano, E. Tenjo, H. Takeshita and K. Kishi, *Anal. Biochem.*, 1992, **206**, 172–177.
11 J. S. Roth and S. W. Milstein, *J. Biol. Chem.*, 1952, **196**, 489–498.
12 T. Greiner-Stoeffele, M. Grunow and U. Hahn, *Anal. Biochem.*, 1996, **240**, 24–28.
13 C. Tong, C. Zhao, B. Liu, B. Li, Z. Ai, J. Fan and W. Wang, *Anal. Chem.*, 2018, **90**, 2655–2661.
14 J. Du, Y. Dong, H. Liu, L. Gong, S. Lu, C. Yang and Y. Li, *Microchem. J.*, 2019, **147**, 842–847.
15 J.-W. Choi, B. M. Krishna Vasamsetti, K.-W. Kim, S. Hwan Seo, D.-H. Lee, S.-I. Chang, J. Choo and H. Yong Kim, *Analyst*, 2017, **142**, 2329–2336, DOI: 10.1039/C6AN02724E.
16 C. Zhao, S. Liu, W. Dang, Q. Liu, D. Yin, B. Liu and C. Hou, *Anal. Chem.*, 2025, **97**, 16690–16697.
17 J. R. Glass, J. C. Dickerson and D. A. Schultz, *Anal. Biochem.*, 2006, **353**, 209–216.
18 D. Li, E. Yang, Z. Luo, Q. Xie and Y. Duan, *Nanoscale*, 2021, **13**, 2492–2501.
19 L. Xu, J. Duan, J. Chen, S. Ding and W. Cheng, *Anal. Chim. Acta*, 2021, **1148**, 238187.
20 L. Gu, W. Yan, L. Liu, S. Wang, X. Zhang and M. Lyu, *Pharmaceuticals*, 2018, **11**, 35.
21 D. Chang, J. Li, R. Liu, M. Liu, K. Tram, N. Schmitt and Y. Li, *Angew. Chem. Int. Ed.*, 2023, **62**, e202315185.
22 W. Kang, F. Xiao, X. Zhu, X. Ling, S. Xie, R. Li, P. Yu, L. Cao, C. Lei, Y. Qiu, T. Liu and Z. Nie, *Angew. Chem. Int. Ed.*, 2024, **63**, e202400599.
23 Z. Mao, R. Chen, X. Wang, Z. Zhou, Y. Peng, S. Li, D. Han, S. Li, Y. Wang, T. Han, J. Liang, S. Ren and Z. Gao, *Trends Food Sci. Technol.*, 2022, **122**, 211–222.
24 J. H. Jeung, H. Han, C. Y. Lee and J. K. Ahn, *Biosensors*, 2023, **13**, 963.
25 X. Zhang, S. Liu, X. Song, H. Wang, J. Wang, Y. Wang, J. Huang and J. Yu, *ACS Sens.*, 2019, **4**, 2140–2149.
26 Y. Roupioz, *J. Chem. Educ.*, 2019, **96**, 1002–1007.
27 J. Li, F. Liu, Z. Zhu, D. Liu, X. Chen, Y. Song, L. Zhou and C. Yang, *ACS Appl. Mater. Interfaces*, 2018, **10**, 13390–13396.
28 Z. Wang, A. Zhang, P. Chang, Y. Shi and Z. Li, *Opt. Fiber Sens. Technol.*, 2025, **91**, 104148.
29 H. Xiong, R. Qiang, K. Ying, D. Xia, S. Li, L. Hao and X. Zheng, *Microchem. J.*, 2025, 116469.
30 N. Kumari, A. Kumar and R. Prakash, *Microchem. J.*, 2025, **212**, 113507.
31 R. Wang, R. Yu, Z. Wang, Q. Zhu and Z. Dai, *Sci. China: Chem.*, 2020, **63**, 860–864.
32 Y. L. Jung, C. Y. Lee, J. H. Park, K. S. Park and H. G. Park, *Nanoscale*, 2018, **10**, 4339–4343.
33 S. Munusamy, H. Zheng, R. Jahani, S. Zhou, J. Chen, J. Kong and X. Guan, *ACS Appl. Bio Mater.*, 2025, **8**, 754–762.
34 S. Liu, T. Xie, X. Pei, S. Li, Y. He, Y. Tong and G. Liu, *Sens. Actuators, B*, 2023, **377**, 133009.
35 Y. Huang, T. Yin, Y. Wen, S. Qian, Y. Wu, X. Hao, W. Chen, B. Li, Z. Li, S. Ramadan and L. Xu, *Moore More*, 2025, **2**, 17.

36 S. Munusamy, R. Jahani, H. Zheng, J. Chen, J. Kong, Y. Zhao, L. Guan, S. Zhou and X. Guan, *ACS Appl. Bio Mater.*, 2025, **8**, 10818–10826.
37 S. Munusamy, H. Zheng, R. Jahani, S. Zhou, J. Chen, J. Kong and X. Guan, *Anal. Bioanal. Chem.*, 2024, **416**, 6985–6994.
38 J. Shendure, S. Balasubramanian, G. M. Church, W. Gilbert, J. Rogers, J. A. Schloss and R. H. Waterston, *Nature*, 2017, **550**, 345–353.
39 G. M. Roozbahani, Y. Zhang, X. Chen, M. H. Soflaee and X. Guan, *Analyst*, 2019, **144**, 7432–7436.
40 Y. Han, S. Zhou, L. Wang and X. Guan, *Electrophoresis*, 2015, **36**, 467–470.
41 Q. Zhao, R. S. S. de Zoysa, D. Wang, D. A. Jayawardhana and X. Guan, *J. Am. Chem. Soc.*, 2009, **131**, 6324–6325.
42 M.-Y. Li, H. Niu, J. Jiang, X.-Y. Wu, Y.-L. Ying and Y.-T. Long, *J. Am. Chem. Soc.*, 2025, **147**, 17121–17131.
43 H. Zheng, S. Munusamy, S. Zhou, R. Jahani, J. Chen, J. Kong and X. Guan, *Small*, 2025, **21**, 2407184.
44 H. Zheng, S. Munusamy, S. Zhou, A. Kanaheraarachchi, J. Kong, J. Chen, R. Jahani, Y. Zhao and X. Guan, *Small Methods*, 2026, **10**, e01003.
45 H. Zheng, S. Munusamy, R. Jahani and X. Guan, *Talanta*, 2024, **276**, 126276.
46 R. Jahani, S. Munusamy, H. Zheng, J. Kong, J. Chen, S. Zhou and X. Guan, *ACS Chem. Neurosci.*, 2025, **16**, 2844–2853.
47 C. McVey, F. Huang, C. Elliott and C. Cao, *Biosens. Bioelectron.*, 2017, **92**, 502–508.
48 J. Chen, S. Munusamy, R. Jahani, R. Guan, H. Zheng, S. Zhou, J. Kong, Y. Zhao, L. Guan, A. Kanaherarachchi and X. Guan, *ACS Meas. Sci. Au*, 2025, **5**, 942–950.
49 Y. Zhang, X. Chen, S. Yuan, L. Wang and X. Guan, *Anal. Chem.*, 2020, **92**, 15042–15049.